INVESTIGATIONS ON ENTROPY LAYER ALONG HYPERSONIC HYPERBOLOIDS USING A DEFECT BOUNDARY LAYER

J. Ph. Brazier, B. Aupoix and J. Cousteix
ONERA/CERT – Département Aérothermodynamique
2 Avenue E. Belin B.P. 4025
31055 Toulouse Cedex (France)

Abstract

A defect approach coupled with matched asymptotic expansions is used to derive a new set of boundary layer equations. This method ensures a smooth matching of the boundary layer with the inviscid solution. These equations are solved to calculate boundary layers over hypersonic blunt bodies, involving the entropy gradient effect. Systematic comparisons are made for both axisymmetric and plane flows in several cases with different Mach and Reynolds numbers. After a brief survey of the entropy layer characteristics, the defect boundary layer results are compared with standard boundary layer and full Navier-Stokes solutions. The entropy gradient effects are found to be more important in the axisymmetric case than in the plane one. The wall temperature has a great influence on the results through the displacement effect. Good predictions can be obtained with the defect approach over a cold wall in the nose region, with a first order solution. However, the defect approach gives less accurate results far from the nose on axisymmetric bodies because of the thinning of the entropy layer.

Introduction

A blunt body in hypersonic flow is preceded by a bow shock wave, detached in front of the nose. This strong curved shock wave induces an entropy gradient in the shock layer. For an inviscid flow, the entropy gradient is related to the vorticity through Crocco equation :

$$\overrightarrow{\text{curl}}\ \vec{V} \wedge \vec{V} = -\overrightarrow{\text{grad}}\ H_t + T\ \overrightarrow{\text{grad}}\ S$$

Therefore, velocity and temperature gradients also exist in an inviscid shock layer. The standard boundary layer theory of Prandtl cannot take into account normal gradients outside of the boundary layer. Van Dyke proposed an enlarged theory called higher-order boundary layer theory based on matched asymptotic expansions for high Reynolds numbers [11, 12]. Two expansions corresponding to different approximations of the Navier-Stokes solutions are built. One of them called outer expansion is valid far from the wall, where the viscous effects are negligible. The other one called inner expansion describes the boundary layer where the viscous effects are dominating. The Prandtl boundary layer equations then represent the first term of an expansion in powers of a small parameter. The external flow normal gradients are accounted for in the second order term, which is a small perturbation of the first order solution. Several other second order effects, like the wall curvature, the displacement or the rarefied gas effects are brought into evidence. The main advantage of this systematic method is to give not only the equations but also the matching conditions between the different zones.

For hypersonic reentry flows, the Reynolds number is often moderate at high altitudes, because of the low density of air. The boundary layers are thus thick and can be of the same order of magnitude as the entropy layer, and the inviscid flow quantities can undergo important variations between the wall and the edge of the boundary layer. Because of the hypothesis of Reynolds number tending towards infinity, the boundary layer is assumed to be very thin in Van Dyke's theory and the inviscid flow gradients are represented only by their wall value. So the second order expansion cannot ensure a good matching of the boundary layer with the inviscid flow if the inviscid profiles are not linear, and the influence of the external vorticity on the skin friction and the wall heat flux is not correctly estimated.

Defect approach

Decomposition

To ensure a smooth matching at any order whatever the external flow, a defect approach has been used, coupled with asymptotic expansions [3]. In the boundary layer region, the variables are no longer the physical variables, but the difference of them with the external solution (Le Balleur [9]). We consider a steady two-dimensional flow of ideal gas. The variables ρ, u, v, p and T stand for the density, tangential and normal component of the velocity, pressure and temperature. The equations are written in a system of orthogonal curvilinear coordinates (ξ, η) where ξ represents the curvilinear abscissa along the body and η is the distance to the wall. All the variables are made dimensionless by referencing them to the upstream values ρ_∞ and U_∞, the nose radius R_0 and $T_0 = U_\infty^2/C_p$. So we write :

$$\begin{aligned} \rho &= \rho_E + \rho_D \\ u &= u_E + u_D \\ v &= v_E + v_D - v_E(\xi, 0) \\ p &= p_E + p_D \\ T &= T_E + T_D \end{aligned}$$

where the subscript E stands for the external variables and the defect variables are labelled D. The term $v_E(\xi, 0)$ has been added to keep the condition $v_D(\xi, 0) = 0$ at the wall whatever the value of v_E.

Expansions are then written using the same small parameter ε as Van Dyke :

$$\varepsilon = \frac{1}{\sqrt{\text{Re}}} \qquad \text{Re} = \frac{\rho_\infty U_\infty R_0}{\mu(T_0)}$$

The external functions depends on the coordinates (ξ, η). The outer expansions read :

$$u_E(\xi,\eta) = U_1(\xi,\eta) + \varepsilon U_2(\xi,\eta) + \cdots$$
$$v_E(\xi,\eta) = V_1(\xi,\eta) + \varepsilon V_2(\xi,\eta) + \cdots$$
$$p_E(\xi,\eta) = P_1(\xi,\eta) + \varepsilon P_2(\xi,\eta) + \cdots$$
$$\rho_E(\xi,\eta) = R_1(\xi,\eta) + \varepsilon R_2(\xi,\eta) + \cdots$$
$$T_E(\xi,\eta) = T_1(\xi,\eta) + \varepsilon T_2(\xi,\eta) + \cdots$$

In the inner region, a stretched normal coordinate $\bar{\eta} = \eta/\varepsilon$ is used for the defect variables :

$$u_D(\xi,\eta) = u_1(\xi,\bar{\eta}) + \varepsilon u_2(\xi,\bar{\eta}) + \cdots$$
$$v_D(\xi,\eta) = \varepsilon\bar{v}_1(\xi,\bar{\eta}) + \varepsilon^2\bar{v}_2(\xi,\bar{\eta}) + \cdots$$
$$p_D(\xi,\eta) = p_1(\xi,\bar{\eta}) + \varepsilon p_2(\xi,\bar{\eta}) + \cdots$$
$$\rho_D(\xi,\eta) = \rho_1(\xi,\bar{\eta}) + \varepsilon \rho_2(\xi,\bar{\eta}) + \cdots$$
$$T_D(\xi,\eta) = t_1(\xi,\bar{\eta}) + \varepsilon t_2(\xi,\bar{\eta}) + \cdots$$

The expansion for v must be shifted to avoid the degeneracy of the continuity equation. These expansions are then brought into the Navier-Stokes equations, and terms of like power of ε are equated.

Equations

In the outer region, the defect variables are null and the equations for the outer flow are exactly the same as for Van Dyke's theory, i.e. Euler equations. Concerning the inner region, one must first bring the above expansions into the Navier-Stokes equations, then substract the external equations, and at last equate same powers of ε. For practical convenience, the inner equations can then be rewritten in outer coordinates, using η instead of $\bar{\eta}$, and replacing $\bar{v}_1$ and $\bar{v}_2$ by :

$$v_1(\xi,\eta) = \varepsilon\bar{v}_1(\xi,\bar{\eta}) \qquad v_2(\xi,\eta) = \varepsilon\bar{v}_2(\xi,\bar{\eta})$$

Then the following first-order equations are obtained :

- continuity :

$$\frac{\partial}{\partial\xi}\left[r^j\rho_1 U_1 + r^j(R_1+\rho_1)u_1\right] + \frac{\partial}{\partial\eta}\left[r^j\rho_1(V_1+v_1)\right] + r^j R_1\frac{\partial v_1}{\partial\eta} = 0$$

- ξ-momentum :

$$(R_1+\rho_1)(U_1+u_1)\frac{\partial u_1}{\partial\xi} + \left[\rho_1 U_1 + (R_1+\rho_1)u_1\right]\frac{\partial U_1}{\partial\xi}$$
$$+(R_1+\rho_1)(V_1+v_1)\frac{\partial u_1}{\partial\eta} = -\frac{\partial p_1}{\partial\xi} + \frac{1}{\mathrm{Re}}\frac{\partial}{\partial\eta}\left(\mu_1\frac{\partial u_1}{\partial\eta}\right)$$

- η-momentum :

$$0 = -\frac{\partial p_1}{\partial\eta}$$

- energy :

$$(R_1+\rho_1)(U_1+u_1)\frac{\partial t_1}{\partial\xi} + \left[\rho_1 U_1 + (R_1+\rho_1)u_1\right]\frac{\partial T_1}{\partial\xi}$$
$$+(R_1+\rho_1)(V_1+v_1)\frac{\partial t_1}{\partial\eta} = u_1\frac{\partial P_1}{\partial\xi} + (U_1+u_1)\frac{\partial p_1}{\partial\xi}$$
$$+\frac{\partial}{\partial\eta}\left(\frac{\mu_1}{\mathrm{Pr}\,\mathrm{Re}}\frac{\partial t_1}{\partial\eta}\right) + \frac{\mu_1}{\mathrm{Re}}\left(\frac{\partial u_1}{\partial\eta}\right)^2$$

- state :

$$p_1 = \frac{\gamma-1}{\gamma}\left[\rho_1 T_1 + (R_1+\rho_1)t_1\right]$$

The symbol r represents the distance from the wall to the symmetry axis, with $j = 0$ for plane and $j = 1$ for axisymmetric bodies. As in Prandtl equations, the wall curvature appear in the first-order equations only through the transverse curvature radius in the continuity equation. The second-order equations are small-perturbations of the above ones plus source terms due to curvature effects, like in Van Dyke theory.

Matching conditions

Each expansion must satisfy the boundary conditions corresponding to its own validity domain. The upstream conditions are to be applied to the outer expansion and the wall conditions to the inner one. The missing conditions are obtained by matching the inner and outer expansions. At the edge of the boundary layer, we can write :

$$u \to u_E$$
$$v \to v_E$$
$$\rho \to \rho_E$$
$$p \to p_E$$
$$T \to T_E$$

and so for the defect variables :

$$u_D \to 0$$
$$v_D \to v_E(\xi,0)$$
$$\rho_D \to 0$$
$$p_D \to 0$$
$$T_D \to 0$$

Thus at first order :

$$\lim_{\eta\to\infty} u_1 = 0$$
$$V_1(\xi,0) = 0$$
$$\lim_{\eta\to\infty} p_1 = 0$$
$$\lim_{\eta\to\infty} t_1 = 0$$
$$\lim_{\eta\to\infty} \rho_1 = 0$$

The conditions on p, ρ and T are not independant since they are linked through the state equation. The condition on v is not a boundary condition for the inner expansion but it gives the wall condition for the outer flow.

The wall conditions for the inner flow are :

$$u = U_1 + u_1 + \varepsilon(U_2+u_2) = 0$$
$$v = \varepsilon\bar{v}_1 + \varepsilon^2\bar{v}_2 = 0$$
$$T = T_1 + t_1 + \varepsilon(T_2+t_2) = T_w$$

hence :

$$u_1(\xi,0) = -U_1(\xi,0)$$
$$v_1(\xi,0) = 0$$
$$t_1(\xi,0) = T_w - T_1(\xi,0)$$

Discussion

Thanks to the small perturbation approach, the calculations of external flow and boundary layer are uncoupled and can be performed separately provided that a specified sequence is respected. First order external problem must be solved first, then first order internal, second order external, and so on. The defect boundary layer equations are parabolic and can be solved by space marching at a very low cost, like the standard Prandtl equations.

The conditions at the edge of the boundary layer ensure a smooth merging of the boundary layer into the inviscid flow whatever the inviscid profiles. From a theoretical point of view, it can be shown that the defect expansions are consistent with Van Dyke's ones by the fact that at a given order they differ only by terms which are higher-order in Van Dyke's theory.

Using the above conditions, the first order η-momentum equation reduces to

$$p_1 = 0$$

So, the pressure in the first-order boundary layer is everywhere equal to the local inviscid flow pressure, instead of its wall value like in Van Dyke's theory.

Applications

To experiment the defect approach, several cases have been selected for a blunt body in a hypersonic flow of ideal gas. The general shape of the body is a plane or axisymmetric hyperboloid, defined by the nose radius and the angle of the asymptotes, at zero degree incidence. The numerical data are given by Shinn, Moss and Simmonds [10] for a hyperboloid equivalent to the windward symmetry line of the U.S. space shuttle. Two points of the reentry trajectory of the STS-2 flight are considered here :

Reentry trajectory - Flight STS-2		
Mach M_∞	26.6	23.4
time (s)	250	650
altitude (km)	85.74	71.29
nose radius R_0 (m)	1.322	1.253
asymptotes half-angle (°)	41.7	40.2
pressure p_∞ (Pa)	0.3634	4.0165
temperature T_∞ (K)	199	205
velocity U_∞ (m/s)	7530	6730
density ρ_∞ (kg/m^3)	$6.35\ 10^{-6}$	$6.80\ 10^{-5}$
reference temperature T_0 (K)	56321	44900
Reynolds number $\mathrm{Re} = \frac{\rho_\infty U_\infty R_0}{\mu(T_0)}$	183.55	1865.65
small parameter $\varepsilon = \mathrm{Re}^{-1/2}$	0.074	0.023
Reynolds number $\mathrm{Re}_\infty = \frac{\rho_\infty U_\infty R_0}{\mu_\infty}$	4792	42374

The Prandtl number is assumed to be constant and equal to 0.725. The ratio of specific heats γ is 1.4. The wall temperature is fixed and equal to 1500 K. The viscosity law is Sutherland's. No comparison with experimental data is possible since the real gas effects are not yet included. So Navier-Stokes solutions [8] have been taken as reference, to compare the two Euler + boundary layer methods. Euler calculations are made with a code from ONERA [14]. Standard boundary layer solutions are obtained using a program developed in DERAT [2]. Only first-order boundary layer are presented here since second-order outer flow solutions are not yet available. Several second-order calculations using Van Dyke's theory have been made on a hypersonic blunt body [1, 4, 5, 6, 7].

Axisymmetric hyperboloid

Past a hyperboloid, the shock wave curvature decrease fastly and the entropy field tends to be uniform, except for the streamlines near the wall, which crossed the strongly curved shock wave at the nose. In this case, the entropy layer is characterized by a non-zero normal gradient at the wall and a decreasing thickness towards the rear, since the mass-flow is constant in the entropy layer and the circumference of the body increases (fig. 1 left). The entropy values at the wall and at the edge of the entropy layer remain constant because the wall is a streamline and outside of the entropy layer the flow is isentropic. So the normal entropy gradient at the wall deeply increases downstream. The shock layer is thinner than in the plane case. Far from the nose, the flow is similar to a flow past a sharp cone except in the entropy layer, whose aspect is quite similar to a viscous boundary layer (fig. 2).

Boundary layer profiles are displayed on figures 4 to 7 for the Mach 23.4 case. Longitudinal velocity profiles are plotted on figure 4 at a distance of nine nose radius from the stagnation point. One can see on this figure the important velocity gradient at the wall in the inviscid flow. This gradient diminishes distinctly between the wall and the boundary layer edge. So even with a second-order expansion, Van Dyke's method could not give a good matching, since it considers only the wall value of the gradient. In this case, it would widely overestimate the skin friction (Adams [1]). Due to the very low wall temperature compared to the inviscid flow one, the displacement effect is quasi-null and the Navier-Stokes solution recasts exactly the inviscid profile in the outer region. In this case, the agreement is quite good with the first-order defect boundary layer. A composite profile has been plotted also, using the additive composite expansion (Van Dyke [13]) constructed with the first order inner and outer expansions. It gives good results for the longitudinal velocity, slightly different of the defect ones.

The corresponding profiles for the temperature are shown on figure 5. The defect profile is in rather good agreement with the Navier-Stokes solution, but in this case the composite expansion written with Van Dyke's first order solutions gives very bad results and does not improve the inner solution. This is due to the negative slope at the wall for the inviscid temperature. Figures 6 and 7 show the velocity and temperature profiles at twenty-one nose radius. The growing boundary layer has overlapped a larger part of the entropy layer. Because of the constant total enthalpy, the positive velocity gradient at the wall induces a negative temperature gradient. In spite of this, the wall heat flux is increased by the vorticity, as well as the skin friction, as can be seen on the figures 8 and 9. But the increase is far more important for the wall friction than for the flux. The defect approach underestimates slightly these quantities but gives better predictions than the standard boundary layer.

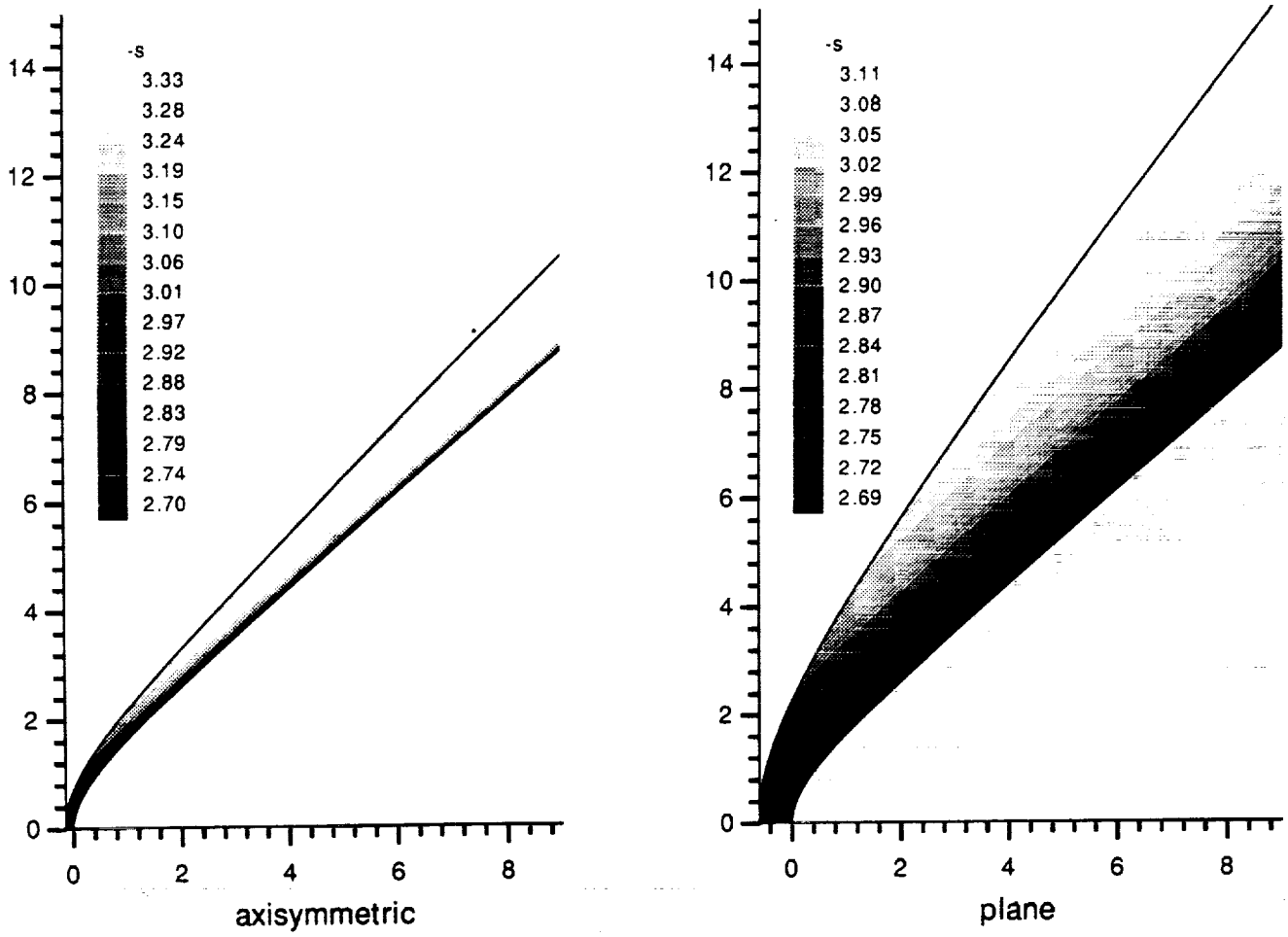

Figure 1: Entropy level in the shock layer – Mach 23.4

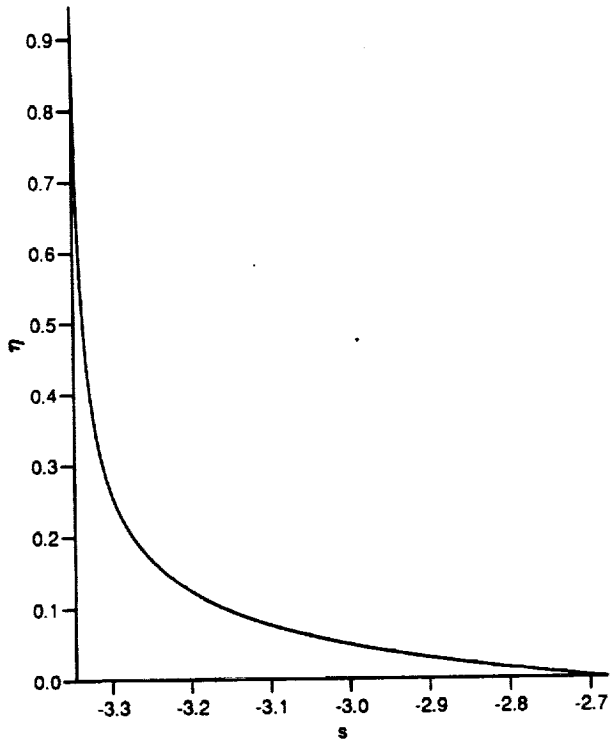

Figure 2: Entropy profile – axisymmetric case Mach 23.4, $\xi = 9$

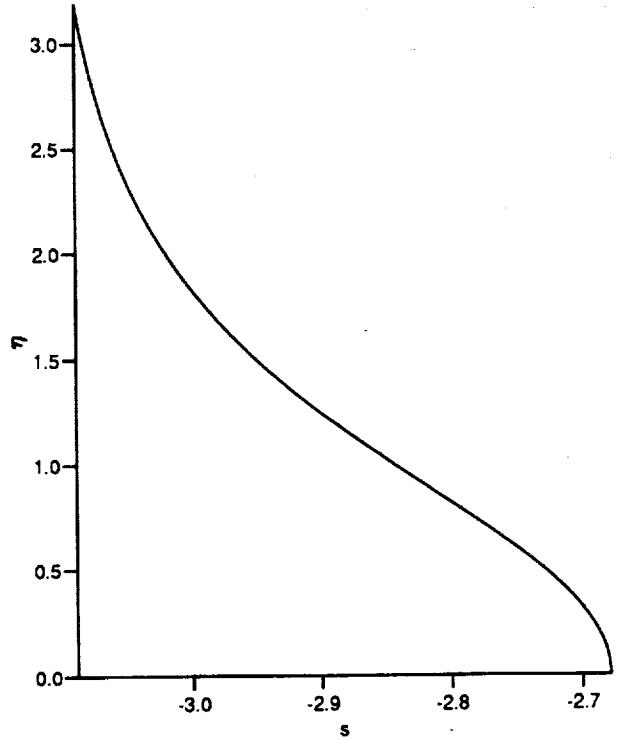

Figure 3: Entropy profile – plane case Mach 23.4, $\xi = 9$

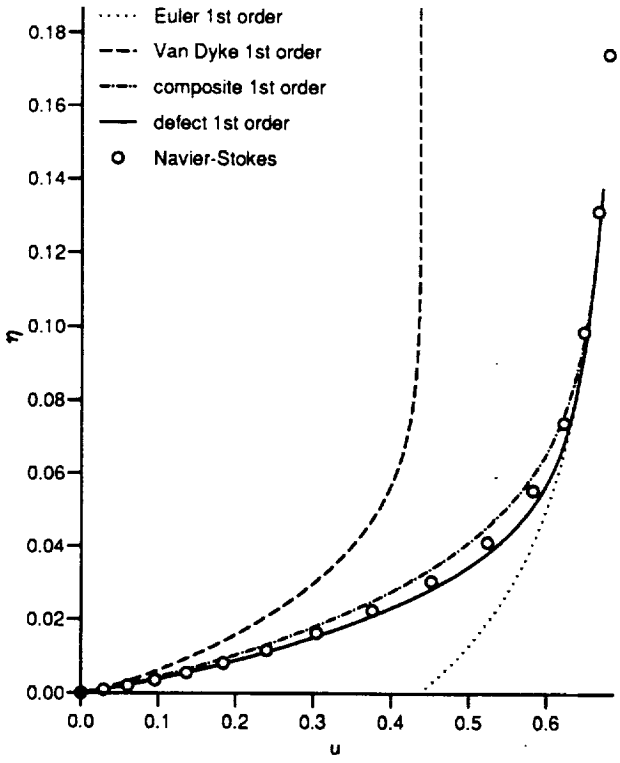

Figure 4: Longitudinal velocity profiles
Mach 23.4, $T_w = 1500$ K, $\xi = 9$

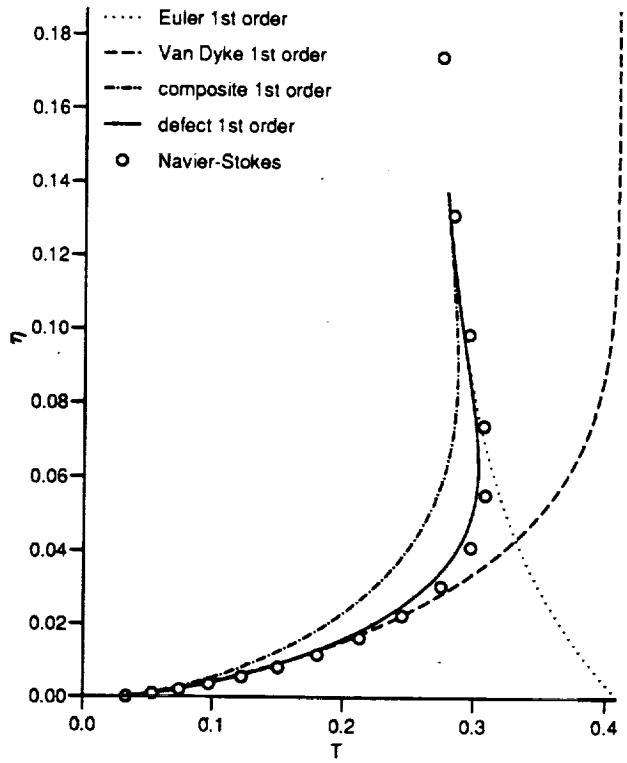

Figure 5: Temperature profiles
Mach 23.4, $T_w = 1500$ K, $\xi = 9$

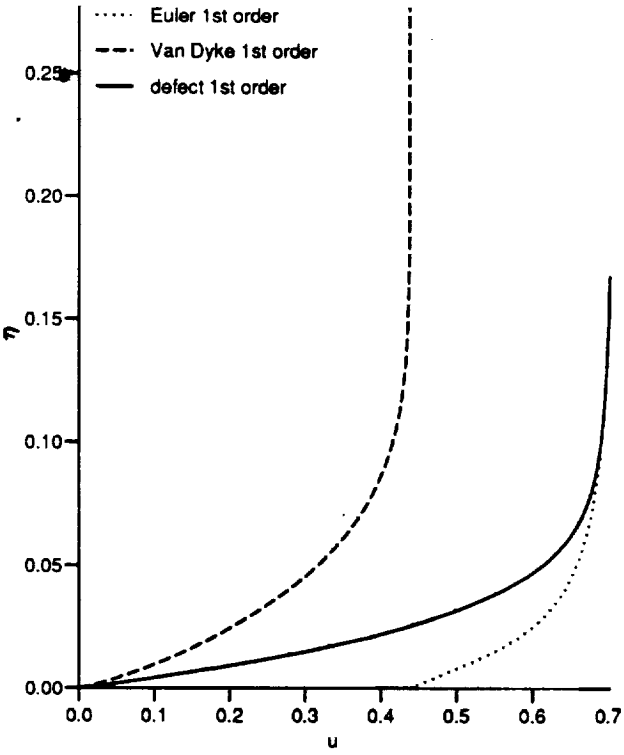

Figure 6: Velocity profiles Mach 23.4, $T_w = 1500$ K, $\xi = 21$

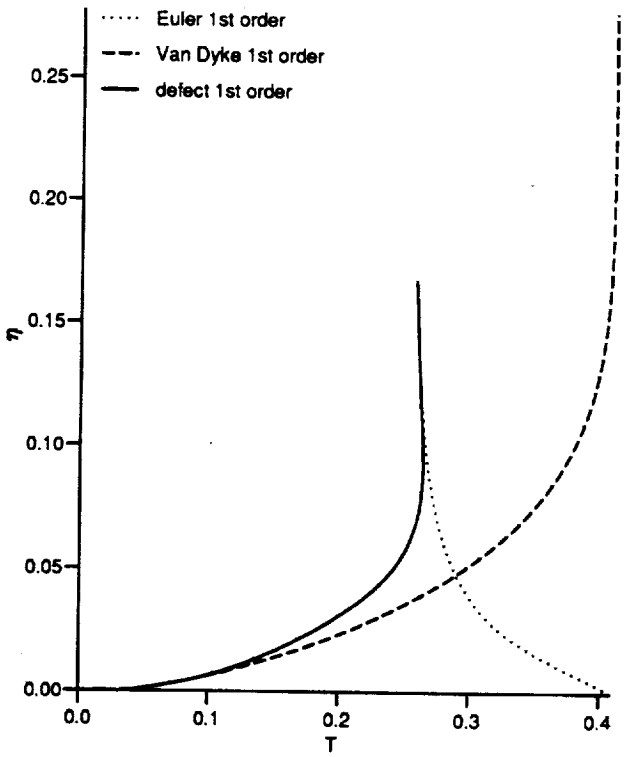

Figure 7: Temperature profiles
Mach 23.4, $T_w = 1500$ K, $\xi = 21$

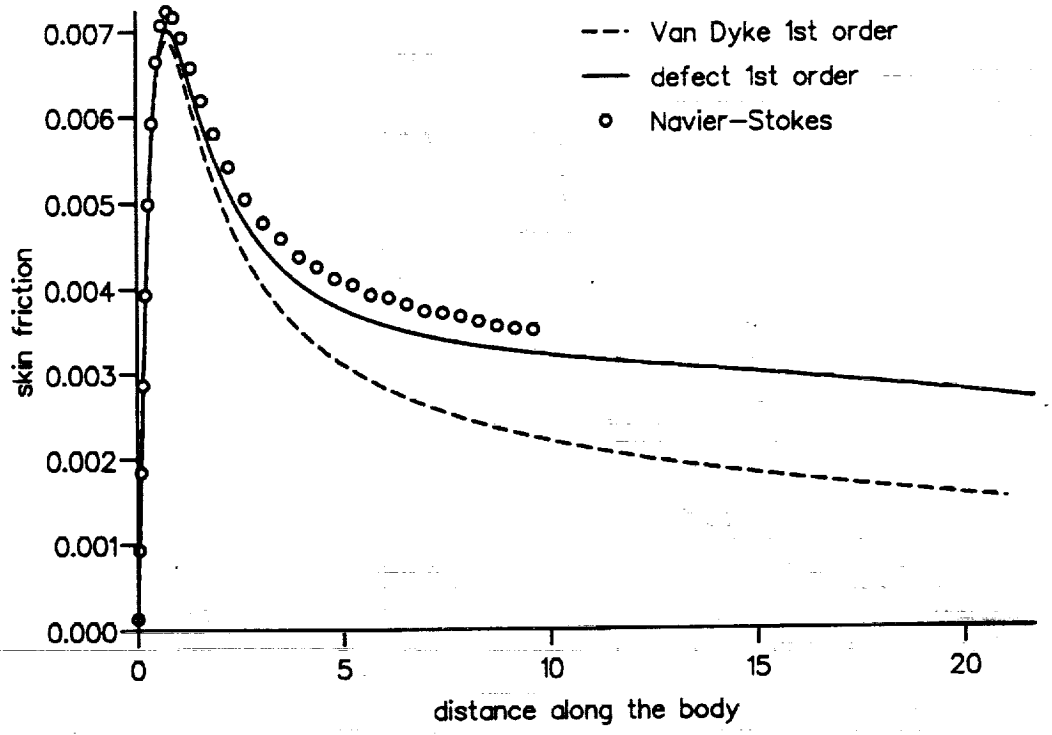

Figure 8: Skin friction on the hyperboloid – Mach 23.4, T_w = 1500 K

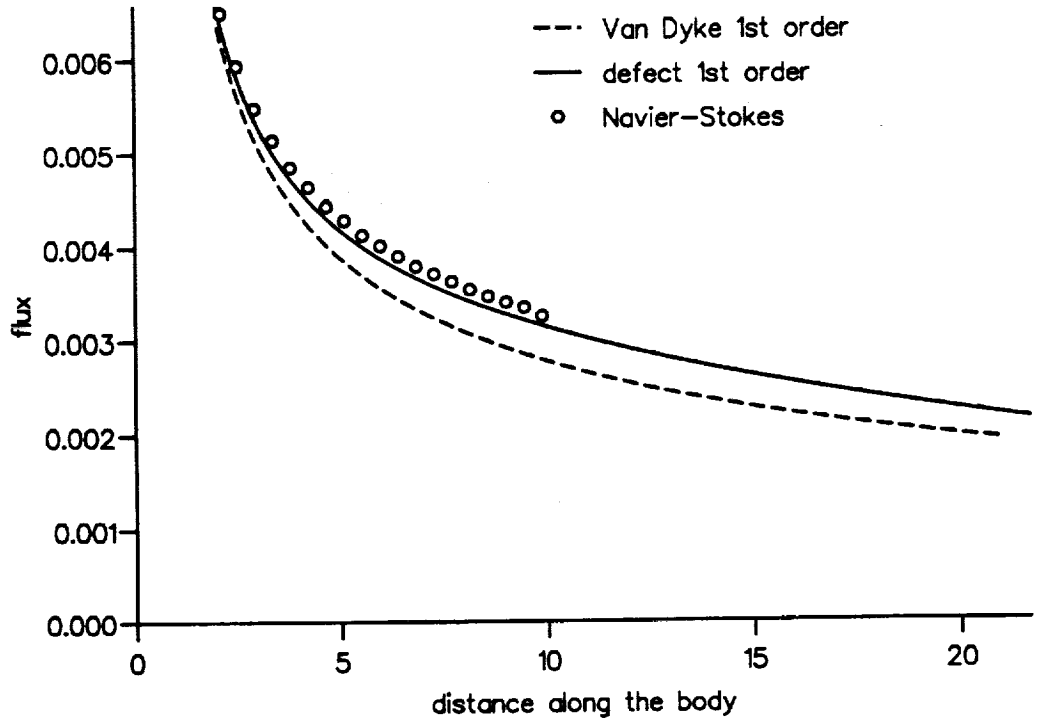

Figure 9: Wall heat flux on the hyperboloid – Mach 23.4, T_w = 1500 K

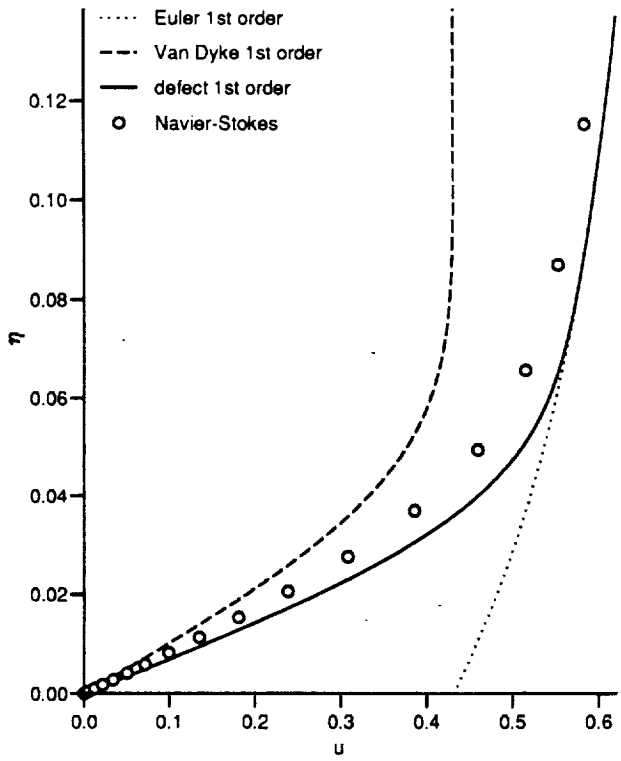

Figure 10: Longitudinal velocity profiles
Mach 23.4, $T_w = 15000$ K, $\xi = 4$

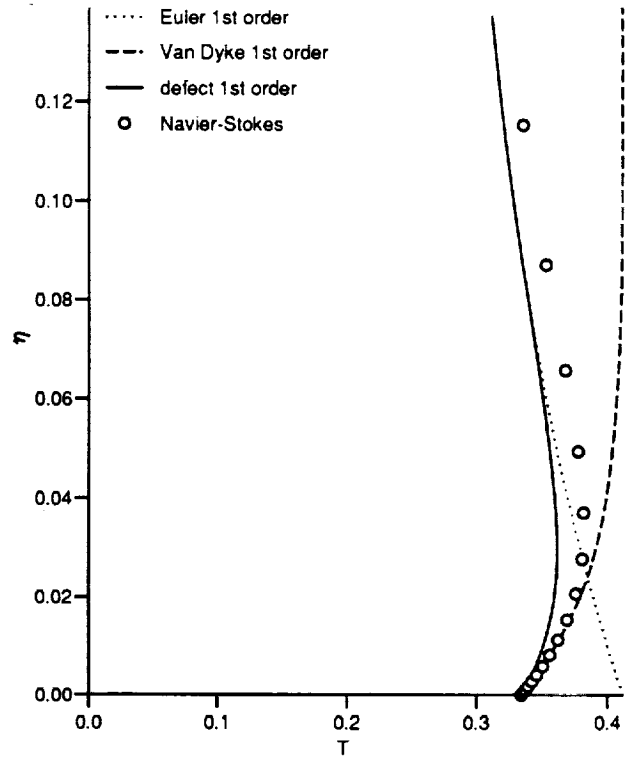

Figure 11: Temperature profiles
Mach 23.4, $T_w = 15000$ K, $\xi = 4$

Figures 10 and 11 show the velocity and temperature profiles with an arbitrary temperature of ten times the temperature of the preceding case. The displacement effect is then far more important and it is obvious on these figures that the Navier-Stokes solution is shifted from the Euler solution in the outer zone. So the first-order boundary layer methods give poor results and a second-order calculation seems to be necessary.

The velocity and temperature profiles at nine nose radius abscissa in the Mach 26.6 case are presented on figures 12 and 13. Because of the lower density, the Reynolds number is small and the boundary layer is about twice as thick as in the Mach 23.4 case. So a large part of the entropy layer is overlapped by the boundary layer. The inviscid velocity and temperature gradients at the edge of the boundary layer are far weaker than their wall values. Due to the high value of the expansion parameter ε, the second order effects are more important and a slight displacement effect is visible between the Euler and Navier-Stokes profiles outside the boundary layer. The agreement between the Navier-Stokes and defect profiles is rather good, but the shear at the wall is a bit too high for the later one. Note that because of the negative inviscid temperature gradient at the wall, the Van Dyke's composite expansion gives again poor results on the temperature profile.

Figures 14 and 15 show the same quantities at twenty-one nose radius from the nose. The entropy layer is now completely included into the boundary layer, and the gradients in the entropy layer become higher than those of the viscous boundary layer. So the hypothesis of neglecting the viscous effects in the external flow does not hold any longer and the defect boundary layer probably gives overestimated values for the slope at the wall of the velocity profile. But no Navier-Stokes solution is yet available on such a large domain.

The corresponding skin friction and wall heat flux are shown on figures 16 and 17. As forecast from the velocity profiles, the defect approach improves greatly the standard boundary layer result, but widely overestimates the skin friction on the rear of the body. The predictions concerning the wall heat flux seem to be more reliable.

Plane hyperbola

Let us now consider a plane hyperbola in the same conditions of hypersonic flows. On figure 1-right are displayed the entropy levels in the inviscid shock layer. The main difference with the axisymmetric case is that now the entropy gradient is null at the wall (Van Dyke [12]). Figure 3 shows entropy profile across the shock layer. The entropy gradient layer is thus located at a short distance above the wall. So the velocity and temperature gradients in the inviscid flow are null at the wall as well, and their influence will be significant only with a very thick boundary layer. Moreover, far downstream, the flow can be assimilated to a parallel flow and the entropy layer's thickness remains constant whereas in the axisymmetric case the entropy layer gets thinner towards the rear part of the body. Thus the entropy gradient remains bounded. Since it is null at the wall, its influence on the skin friction and the heat flux will now be far less important.

On figures 18 and 19 are plotted the velocity and temperature profiles on the Mach 23.4 hyperbola at nine nose radius abscissa. The inviscid gradients are hardly visible outside the boundary layer and all the methods give the same results.

When the Reynolds number is lower, the matching of the

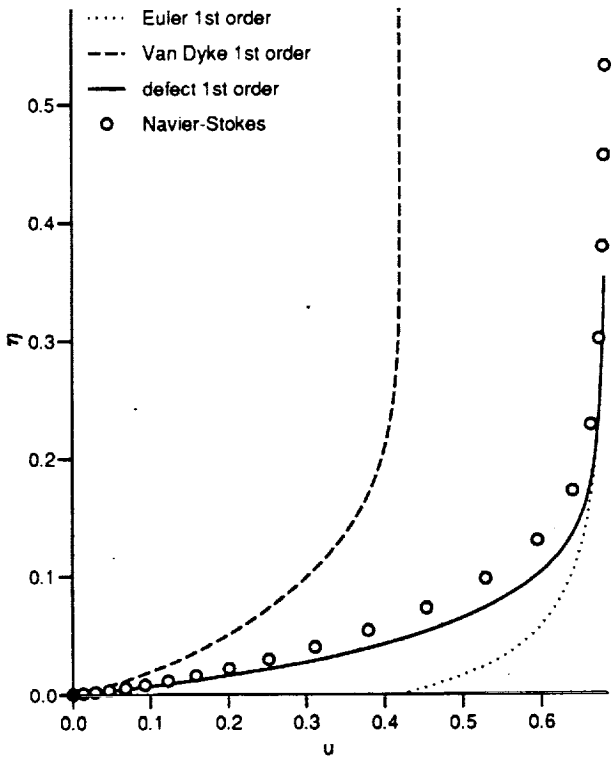

Figure 12: Longitudinal velocity profiles
Mach 26.6, T_w = 1500 K, ξ = 9

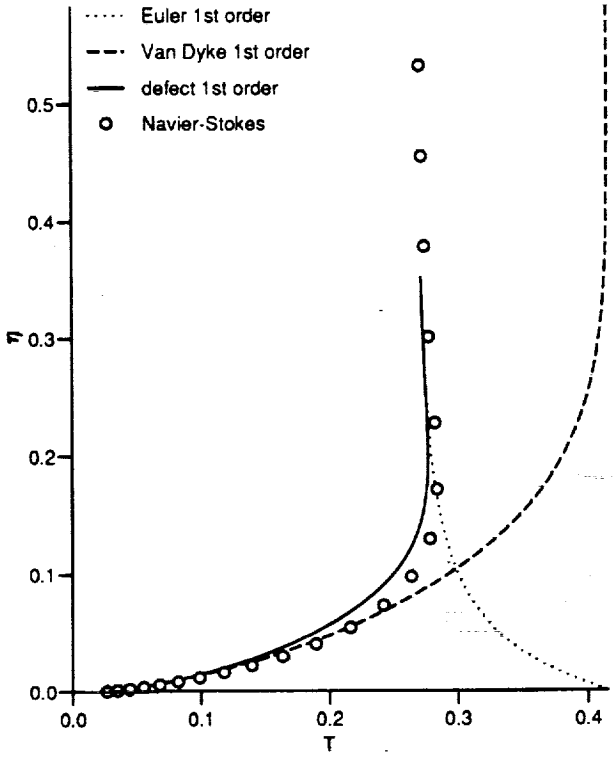

Figure 13: Temperature profiles
Mach 26.6, T_w = 1500 K, ξ = 9

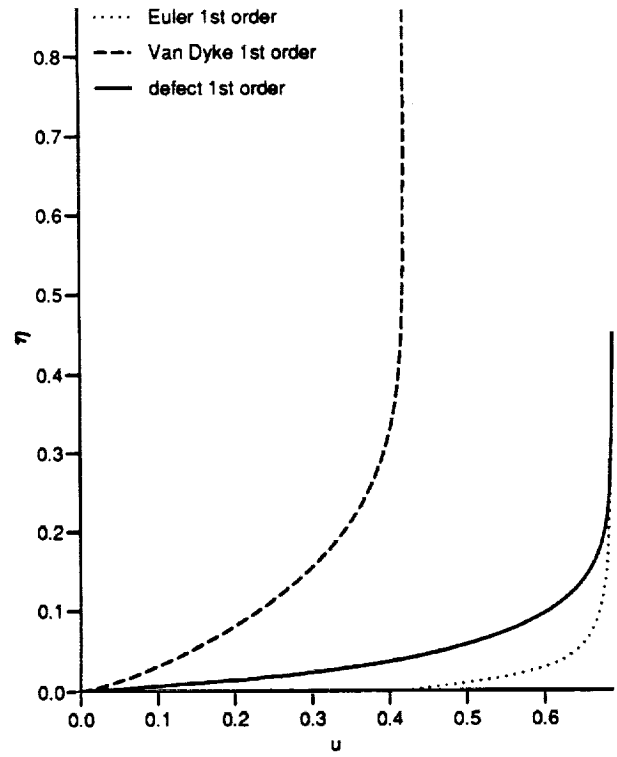

Figure 14: Longitudinal velocity profiles
Mach 26.6, T_w = 1500 K, ξ = 21

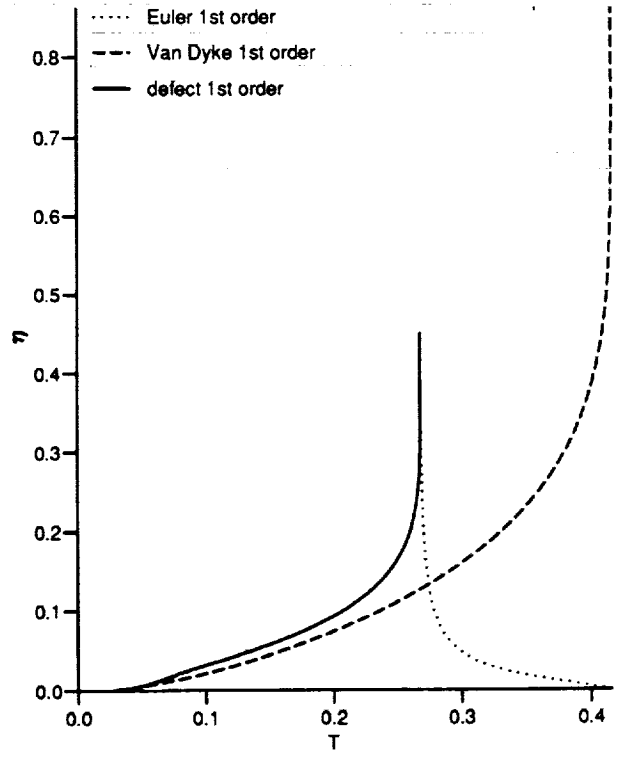

Figure 15: Temperature profiles
Mach 26.6, T_w = 1500 K, ξ = 21

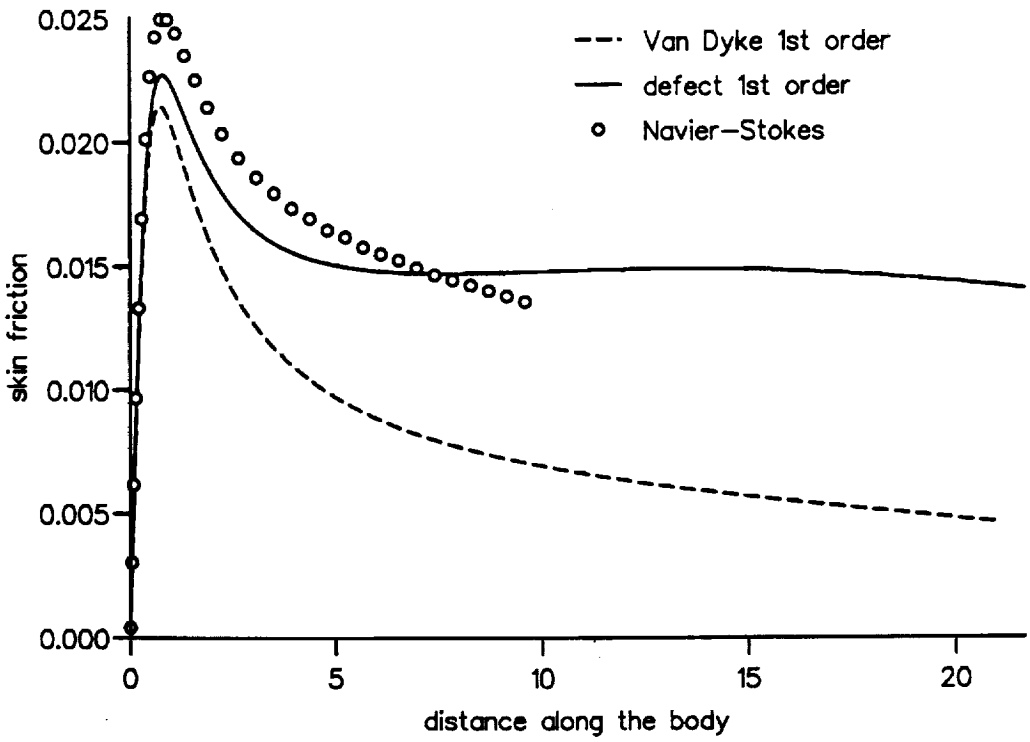

Figure 16: Skin friction on the hyperboloid – Mach 26.6, T_w = 1500 K

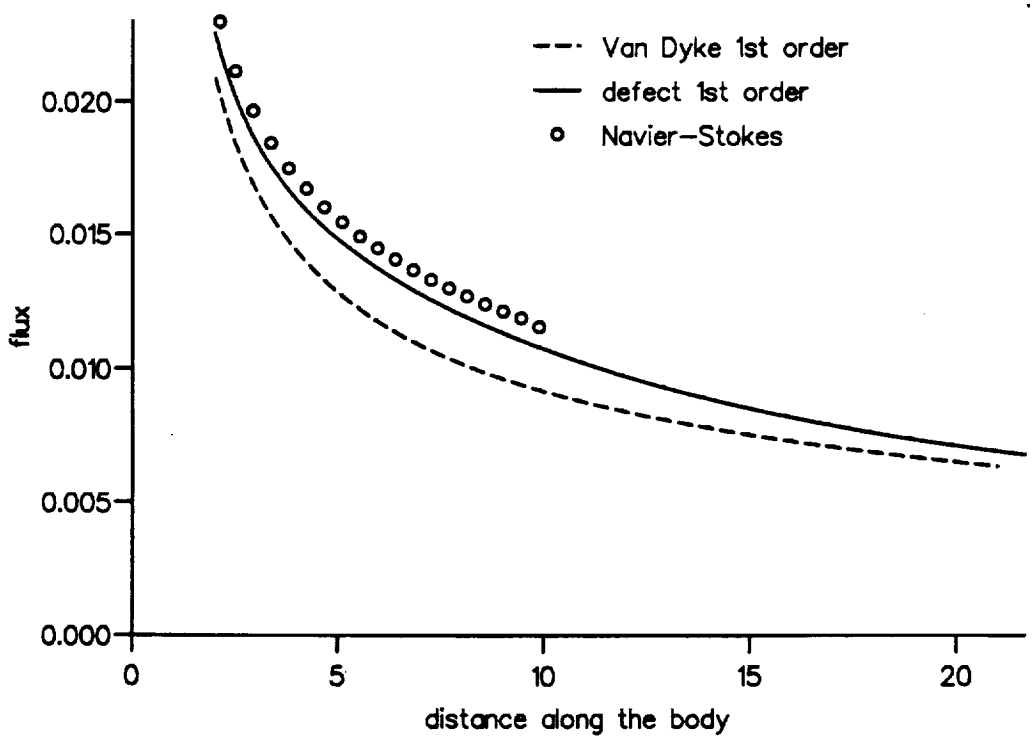

Figure 17: Wall heat flux on the hyperboloid – Mach 26.6, T_w = 1500 K

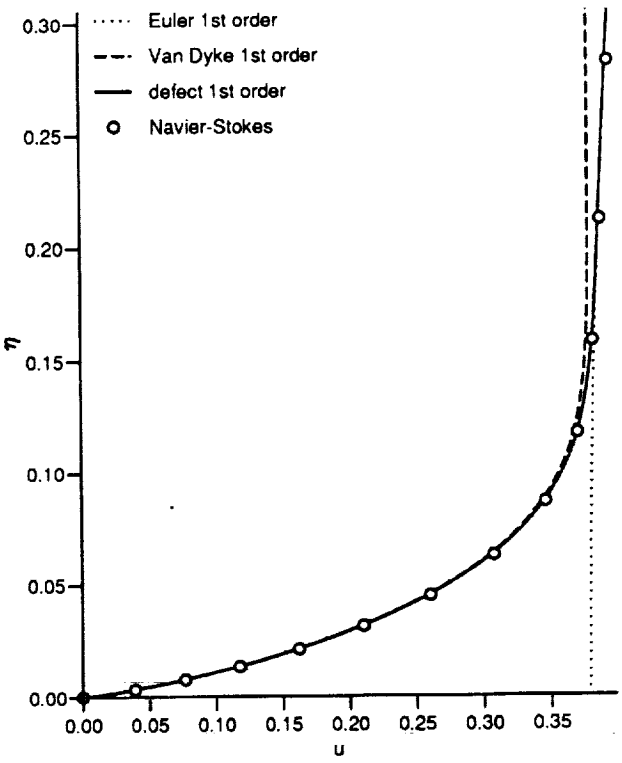

Figure 18: Longitudinal velocity profiles
Mach 23.4, $T_w = 1500$ K, $\xi = 9$

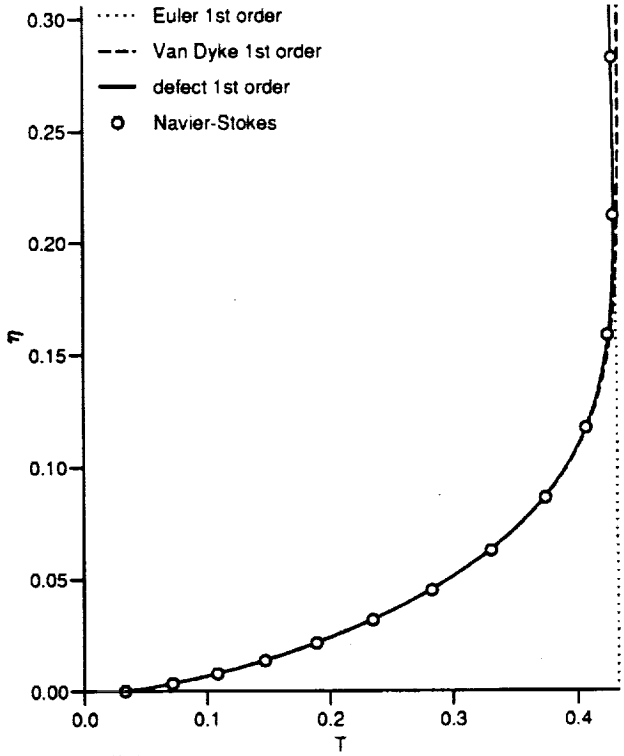

Figure 19: Temperature profiles
Mach 23.4, $T_w = 1500$ K, $\xi = 9$

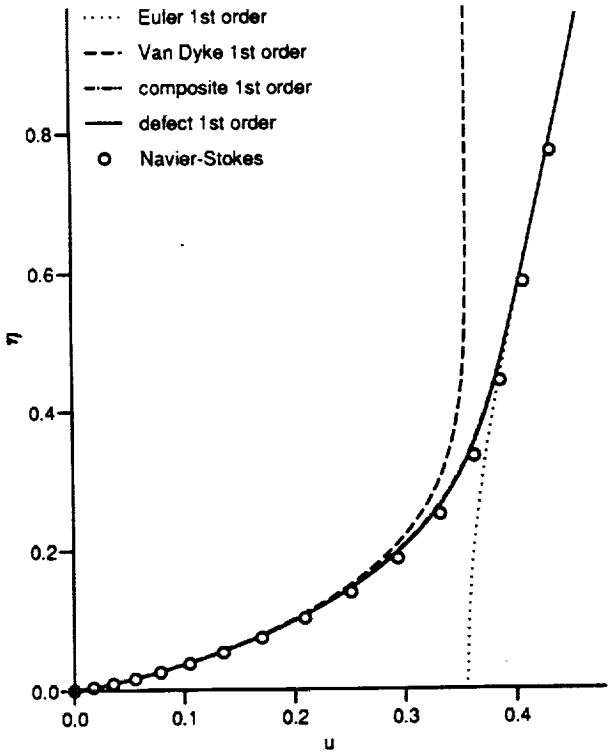

Figure 20: Longitudinal velocity profiles
Mach 26.6, $T_w = 1500$ K, $\xi = 9$

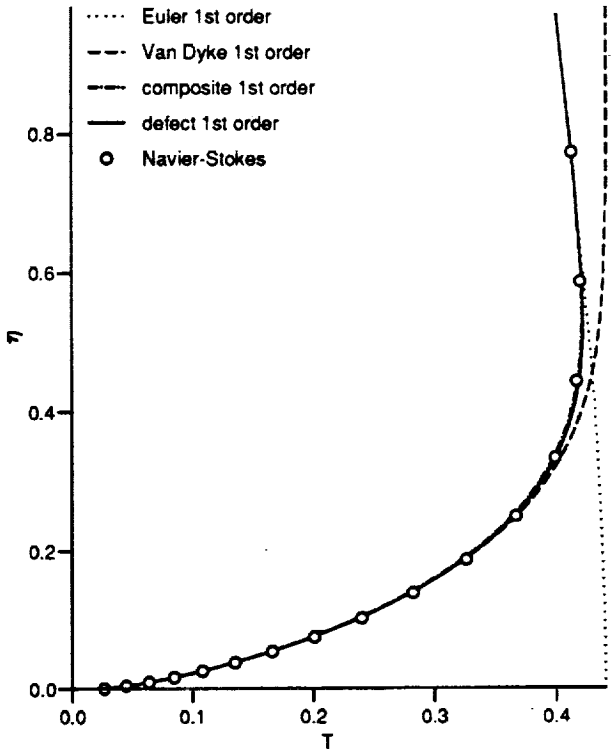

Figure 21: Temperature profiles
Mach 26.6, $T_w = 1500$ K, $\xi = 9$

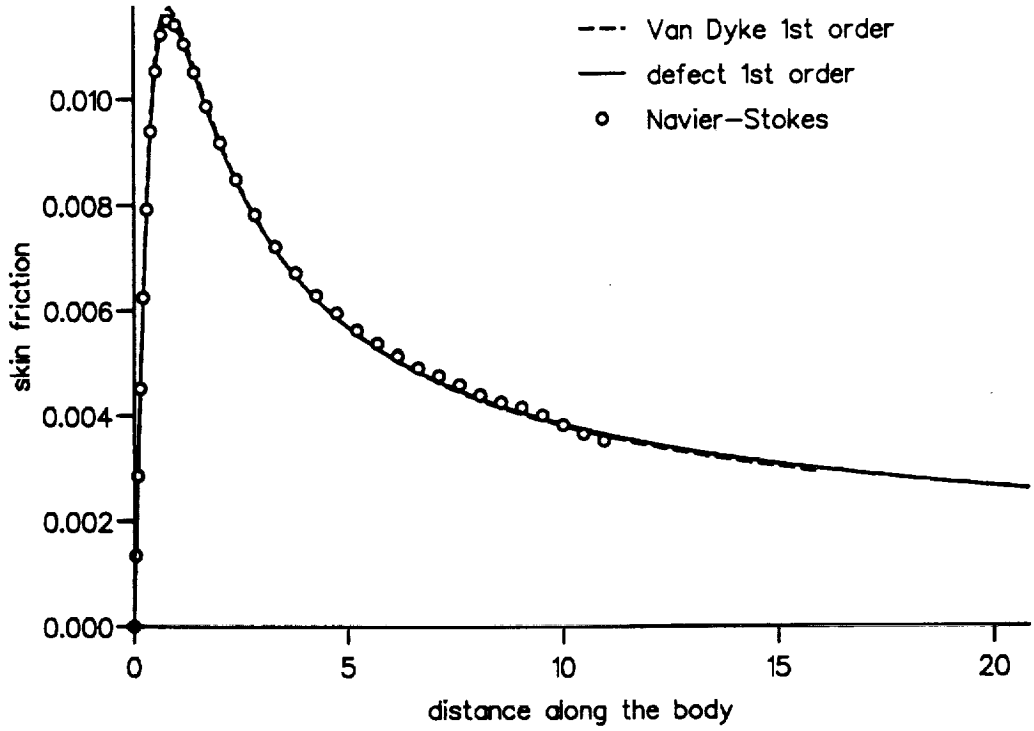

Figure 22: Skin friction on the plane hyperbola - Mach 26.6, T_w = 1500 K

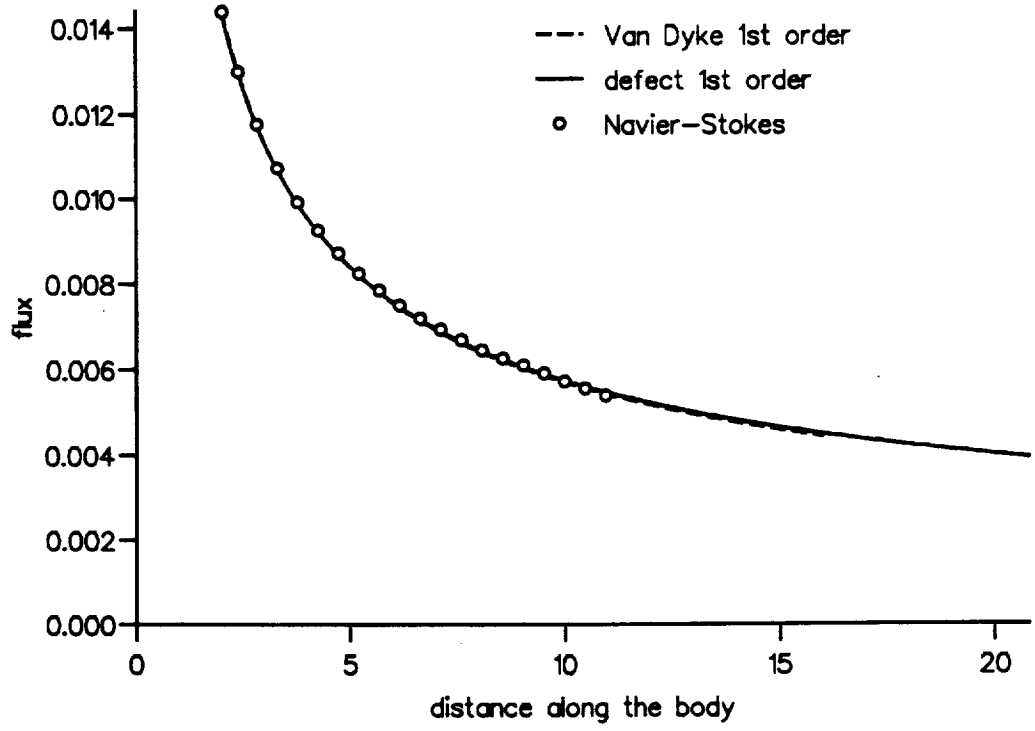

Figure 23: Wall heat flux on the plane hyperbola - Mach 26.6, T_w = 1500 K

boundary layer with the inviscid flow takes place in the gradient region, as can be seen on the figures 20 and 21 for the case Mach 26.6 . The defect method gives a good matching and a correct agreement with Navier-Stokes solutions, but the two boundary layer methods give similar results near the wall. Thus no significant difference is visible on the skin friction and the wall heat flux shown on figures 22 and 23.

Conclusion

Several boundary layer calculations have been performed on various hypersonic bodies, including plane or axisymmetric shapes. The behaviour of the solutions far from the stagnation point has been particularly investigated. The different cases presented here showed both the interest and the limits of boundary layer methods to compute hypersonic flows. Moreover, the importance of taking into account the second order effects when calculating boundary layers at low Reynolds numbers has been brought into evidence. The most important of them are the entropy gradient effect and the displacement effect in the considered cases. They can deeply modify the wall quantities such as the skin friction or the wall heat flux, which are essential to predict the total drag of the vehicle and to design the thermal protection.

Using the matched asymptotic expansions technique, the defect approach allows us to improve the results of the standard higher-order boundary layer theory of Van Dyke, for a similar cost. Particularly, it ensures a smooth matching of the viscous and inviscid flows, even when the inviscid profiles vary significantly through the boundary layer. When the wall temperature is low and thus the displacement effect is negligible, first-order defect calculations can give good results and reproduce Navier-Stokes solutions with a reasonable accuracy at a lower cost, as long as the entropy layer is not too thin compared to the viscous boundary layer. But it gives less accurate results on axisymmetric hyperboloids at low Reynolds number far from the stagnation point, when the inviscid flow normal gradients are higher than those of the boundary layer. The inviscid flow concept seems to be invalid then.

References

[1] J.C. Adams *Higher-order boundary-layer effects on analytic bodies of revolution*, Arnold Engineering Development Center, Report AEDC-TR-68-57 (1968)

[2] B. Aupoix, D. Arnal *CLIC: calcul des couches limites compressibles*, Rapport technique DERAT n° 23/5005.19 (1988)

[3] B. Aupoix, J.Ph. Brazier, J. Cousteix *An asymptotic defect boundary layer theory applied to hypersonic flows* AIAA 91-0026, 29th Aerospace Sciences Meeting, January 7-10, Reno, Nevada (1991)

[4] R.T. Davis, I. Flügge-Lotz *The laminar compressible boundary-layer in the stagnation-point region of an axisymmetric blunt body including the second-order effect of vorticity interaction*, International Journal of Heat and Mass Transfer, Vol. 7, pp. 341-370 (1964)

[5] R.T. Davis, I. Flügge-Lotz *Laminar compressible flow past axisymmetric blunt bodies*, Journal of Fluid Mechanics, Vol. 20, Part 4, pp. 593-623 (1964)

[6] T.K. Fannelöp, I. Flügge-Lotz *Two-dimensional hypersonic stagnation flow at low Reynolds numbers*, Z. Flugwiss. Vol. 13, n° 8, pp. 282-296 (1965)

[7] T.K. Fannelöp, I. Flügge-Lotz *Viscous hypersonic flow over simple blunt bodies; comparison of a second-order theory with experimental results*, Journal de Mécanique, Vol. 5, n° 1, pp. 69-100 (1966)

[8] A. Lafon *Calcul d'écoulements visqueux hypersoniques*, Rapport technique DERAT n° 32/5005.22 (1990)

[9] J.C. Le Balleur *Calcul des écoulements à forte interaction visqueuse au moyen de méthodes de couplage*, AGARD - CP 291 (1980)

[10] J.L. Shinn, J.N. Moss, A.L. Simmonds *Viscous shock layer heating analysis for the shuttle windward plane with surface finite catalytic recombination rates*, AIAA Paper n° 82-0842 (1982)

[11] M. Van Dyke *Higher approximations in boundary layer theory, Part 1: General analysis*, Journal of Fluid Mechanics, vol. 14, pp. 161-177 (1962), *Part 2: Application to leading edges*, Journal of Fluid Mechanics, vol. 14, pp. 481-495 (1962)

[12] M. Van Dyke *Second-order compressible boundary-layer theory with application to blunt bodies in hypersonic flow*, Hypersonic Flow Research, Vol. 7, pp. 37-76 (1962), F.R. Riddell Editor, Academic Press

[13] M. Van Dyke *Perturbation methods in fluid mechanics*, Parabolic Press (1975)

[14] J.P. Veuillot *Calcul de l'écoulement axisymétrique autour d'un corps de rentrée*, Rapport Technique ONERA n° RT 31/1285 AY (Janvier 1989)